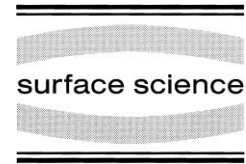




ELSEVIER

Surface Science 465 (2000) 361–371



www.elsevier.nl/locate/susc

Interpreting interfacial structure in cross-sectional STM images of III–V semiconductor heterostructures

B.Z. Nosh, W. Barvosa-Carter, M.J. Yang, B.R. Bennett, L.J. Whitman *

Naval Research Laboratory, Washington, DC 20375, USA

Received 3 May 2000; accepted for publication 18 July 2000

Abstract

Using model GaSb–InAs heterostructures, we have systematically examined how cross-sectional scanning tunneling microscopy (XSTM) can be used for the study of III–V heterostructure interfaces. The interpretation of interfacial structure in XSTM images is impeded by the fact that only every other III or V plane as grown on the (001) substrate is seen in each image. We show how this structural artifact affects spectral analyses of interfacial roughness, preventing an accurate analysis when interfaces are just a few layers wide. Additional complications arise due to the inequivalence of the (110) and (1 $\bar{1}$ 0) cleavage surfaces and the dependence of interfacial bond orientation on growth order. By taking advantage of the different bond orientations on the two cleavage surfaces, we demonstrate that the contrast observed at the interfacial layers in this system is caused primarily by the geometry of the interfacial bonds, not electronic structure differences. Finally, we illustrate how careful design of model heterostructures can be used to circumvent many limitations of XSTM, and thereby allow one to obtain detailed atomic-scale information about all the growth layers in the structure. © 2000 Elsevier Science B.V. All rights reserved.

Keywords: Gallium antimonide; Indium arsenide; Molecular beam epitaxy; Scanning tunneling microscopy; Single crystal epitaxy; Superlattices; Surface structure, morphology, roughness, and topography

1. Introduction

The epitaxial growth of thin film heterostructures inevitably involves the formation of interfaces between layers of different materials. Moreover, as the layer thickness decreases, the fraction of the total structure consisting of interfacial layers increases. Although state-of-the-art epitaxial growth techniques such as molecular beam epitaxy (MBE) can deposit material with sub-monolayer precision, it is challenging nonetheless to create perfectly abrupt interfaces given all the kinetic and thermodynamic factors that influence interface for-

mation. The contributions to interfacial disorder can be separated into two categories: morphological roughness, arising from islands kinetically trapped during growth; and intermixing, observed as compositional fluctuations near the interface associated with segregation. Such interfacial disorder can ultimately impact the electrical and optical device characteristics by affecting transport and scattering mechanisms of carriers across interfaces [1,2], as well as by causing local deviations in the band offsets [3].

During the last decade, cross-sectional scanning tunneling microscopy (XSTM) has emerged as a powerful technique to characterize III–V semiconductor heterostructure interfaces [4–10]. This technique relies on a fortuitous property of the zinc-

* Corresponding author. Fax: +1-202-7673321.

E-mail address: Lloyd.Whitman@nrl.navy.mil (L. Whitman)

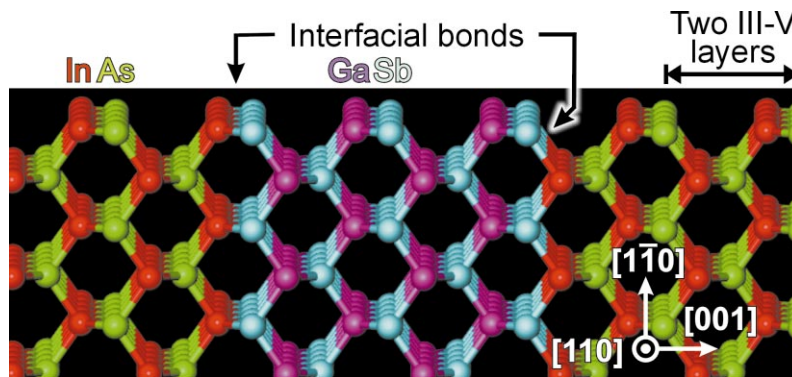


Fig. 1. Ball-and-stick model of an InAs–GaSb–InAs heterostructure with InSb interfacial bonds. The bulk-truncated (110) and ($\bar{1}\bar{1}0$) cleavage surfaces are shown. Note that on relaxed surfaces the exposed III and V atoms move towards and away from the surface, respectively.

blende III–V crystals: they easily cleave along $\{110\}$ crystal faces, producing atomically-abrupt, nearly defect-free surfaces that present a cross-sectional view of structures grown on (001) substrates. Like transmission electron microscopy (TEM), XSTM can be done on samples from any III–V(001) wafer, and can therefore be used to examine the interfaces within samples grown for actual device applications. Accordingly, both techniques can be used to directly correlate interfacial morphology with the electrical and/or optical characteristics of a device. Whereas TEM can examine an interface from any crystallographic direction, and it is a powerful technique for revealing defects in a material, atomic-resolution TEM images present a view averaged through many lattice planes. In contrast, although XSTM is limited to studies of the $\{110\}$ planes, the images show a true cross-section as represented by a *single plane* of atoms. Therefore, XSTM should be an excellent method for studying the atomic-scale structure of heterostructure interfaces. However, a variety of factors must be considered when interpreting interfacial structure from XSTM images, including limitations imposed by both the imaging process itself and the structure of the $\{110\}$ cleavage planes.

2. Limitations of XSTM

In order to discuss the inherent limitations of XSTM, it is useful to review the properties of the

$\{110\}$ cleavage surface. As shown in Fig. 1, there are two possible cleavage planes, exposing either (110) or ($\bar{1}\bar{1}0$) surfaces, that have the same simple surface structure. For example, on the ($\bar{1}\bar{1}0$) face the surface layer consists of ‘zigzag’ chains of alternating III and V atoms running along the [110] direction. It is well established that these III–V surfaces undergo a simple surface relaxation, with the III (V) atoms relaxing towards (away) from the surface, that shifts the electron density between the atoms leaving the III (V) dangling bond essentially empty (filled) [11]. Because STM ‘surface topography’ physically represents contours of constant integrated charge density, this relaxation provides the primary source of contrast in XSTM images: under most imaging conditions, only the III (V) dangling bonds are seen in empty (filled) state constant-current images of III–V $\{110\}$ surfaces.

In XSTM images of heterostructures, the different III–V materials often appear to be at different heights on the $\{110\}$ surface (typically varying by ≤ 0.1 nm). This contrast is generally attributed to differences in electronic structure, such as band gaps, band edge alignments, and/or surface density of states of the materials. Similarly, point defects are often observed that look like individual ‘atoms’ which are slightly raised or depressed in the surface lattice; this contrast has also been attributed to electronic effects. However, because the charge density that determines the STM topography is also a function of the positions

of the surface atoms, local variations in electronic structure cannot be simply distinguished from geometric displacements. For example, variations in topography have been observed that are caused by geometric distortions in the surface plane associated with strain relaxation [12,13]. The convolution between electronic versus geometric contrast can make it challenging to perform an accurate compositional analysis of an interface using XSTM [14].

In addition to the limitations imposed by the imaging process, interfacial analysis by XSTM is also hindered by the zinc-blende crystal structure [15]. Most significantly, the III–V zigzag chains observed in STM images of a {110} surface constitute *every other* III–V layer grown in the [001] direction. The atoms in the alternate layers, below and between each chain, *are not seen*. An important consequence of this limitation is that, for imperfect interfaces, it is impossible to image the actual multilayer profile along the interface. Another complication arises from the inequivalence of the two {110} cleavage surfaces, creating structural differences that are most apparent at the interfaces. Treating the materials in Fig. 1 as InAs (red-green) and GaSb (magenta-cyan), one can see that the InSb (red-cyan) bonds are nominally oriented *in the surface plane* on one cleavage plane, but *out of the plane* on the other (note that on a relaxed surface they may not be strictly orthogonal). This is important because XSTM images only reveal one of the interfacial atoms for the out-of-plane case – the other atom will always be between the rows. Moreover, the bond orientation also depends on the growth order: compare the Sb-on-In bonds on the left with the In-on-Sb bonds on the right. These asymmetries occur in all III–V heterostructures. Further complexity arises for heterostructures without a common anion, such as this one, because two interfacial bond types are possible (GaAs and InSb in this illustration). Similar complications also occur in structures incorporating alloy layers, such as Al(Ga)As/GaAs superlattices, where the atomic scale interfacial structure will be heterogeneous.

The inherent limitations of XSTM for analysis of interfaces at {110} surfaces can be summarized as follows:

1. Only every other III or V plane as grown on the (001) substrate can be observed; depending on the vagaries of the cleavage process, it may *not* be the interfacial plane.
2. Atomic-scale variations in the topography are caused by a convolution of electronic and geometric effects (a generic limitation of STM images).
3. Interfacial bonds may be oriented either into or out of the {110} surface plane depending on the cleave direction.
4. The interfacial bond orientation depends on the heterostructure growth order.

If the actual interfaces are poorly defined due to disorder spanning many growth layers, or only a qualitative characterization of interfacial structure is desired, these limitations will be relatively unimportant. However, when interfacial disorder only occurs within a few growth layers, an accurate, quantitative interpretation of XSTM images will require these factors to be carefully considered. Although some of these issues have been addressed briefly in the past in discussions of specific heterostructures [15], here we systematically explore how best to interpret interfacial structure from XSTM images using model GaSb–InAs heterostructures designed specifically for this purpose.

3. Preparation and imaging of model heterostructures

Model GaSb–InAs heterostructures were grown on GaSb(001) substrates in a solid-source MBE system equipped with cracked arsenic and antimony sources. After desorbing the initial oxide, a $\sim 1 \mu\text{m}$ thick GaSb buffer layer was grown at 500°C , and then the temperature was lowered to $\sim 420^\circ\text{C}$ and the heterostructure was grown. The growth temperatures were determined using reconstruction phase diagrams for GaSb as correlated with Sb flux and infrared transmission thermometry [16,17]. Both GaSb and InAs layers were grown at $0.5 \text{ monolayer (ML) s}^{-1}$ with a V:III flux ratio of $\sim 2:1$ and no intentional doping. Growth rates were calibrated by reflection high-energy electron diffraction (RHEED) intensity oscillations.

In order to make the heterostructures as compositionally abrupt as possible with uniform interfacial bonds, each interface was carefully formed using migration-enhanced epitaxy (MEE) [18,19]. For example, to make a GaSb-on-InAs interface with InSb bonds, 1 ML of In was first deposited on an As-terminated InAs(001)-(2 × 4) surface, followed by a 2 s Sb₂ exposure and then growth of GaSb via co-deposition. For InSb bonds in an InAs-on-GaSb interface, 1 ML of In was first deposited on an Sb-terminated GaSb surface, followed by 2 s of As₂ and then InAs growth. Similarly, GaAs interfacial bonds were made using analogous MEE procedures with alternate Ga and As₂ exposures. Interfacial bonds prepared in this way have previously been shown to be highly uniform as characterized by X-ray diffraction (XRD), Raman spectroscopy, and TEM [18–20].

Samples ca. 4 × 6 × 0.35 mm³ were cut from the substrate wafer and mounted on an STM sample holder, narrow edge-up and with a known orientation. After introducing the samples into the STM vacuum chamber (< 1 × 10⁻¹⁰ Torr), each was out-gassed for 30 min at ~100°C. A sample was then scribed in situ (~1 mm long, perpendicular to the wide edge), and cleaved to expose either a (110) or (1 $\bar{1}$ 0) surface as determined by the initial mounting orientation. Each sample was used only once. Single-crystal tungsten tips were prepared by electrochemical etching, and cleaned in situ by electron bombardment heating prior to use. All images shown here were acquired with constant-current (0.1–0.3 nA) and filled electronic states (2–3 V). Because it is generally easier to obtain high-resolution images of filled electronic states on III–V {110} surfaces, almost all XSTM studies focus on the structure of the group V layers. For this reason, we confine our discussion to interfacial structure as revealed by filled-state images only.

4. The impact of imaging only every-other growth layer

4.1. Identifying the interfacial layer using steps

Although only every other (001) growth layer is exposed on a {110} cleave, there are two types

of step structures that allow one to observe, to some extent, all the layers in cross-section. As shown in Fig. 2, these include *cleavage steps* on the {110} surface caused by an imperfect cleave (Fig. 2a and b), and *growth-layer steps*, present on the (001) surface when an interface is formed and then exposed in cross-section on the {110} surface (Fig. 2c and d).

When a cleavage step on the {110} surface is a single atomic layer high, like the one observed in Fig. 2a, alternate growth layers are exposed on either side of the step, as illustrated in Fig. 2b. In this example the step diagonally crosses a GaSb-on-InAs interface grown with GaAs interfacial bonds. Notice that the rows of As or Sb atoms at the (110) surface shift by half the row spacing on either side of the step, thereby revealing all the group-V layers in the heterostructure. Also note that the row on the right/down side of the step that is between the interfacial Sb and As layers on the left/up terrace has an As-like appearance. Hence, this row must be the *interfacial As* layer (with GaAs bonds), which we denote as the cross-sectional view of growth layer ‘0;’ therefore, the rows above and below it must correspond to the lattice planes two layers above (‘+2’) and below (‘-2’) the interface. Similarly, the interfacial rows exposed on the left/up terrace can then be assigned to the growth planes *one* layer above and below the interface. Even though it is still not possible to observe all the rows in a structure sequentially, cleavage steps at least enable one to definitively identify the actual interfacial layer and thereby analyze the atomic-scale structure as a function of the absolute distance from an interface.

Cleavage steps are not always present and easy to locate, but fortunately the second type of step, a *growth-layer* step, can be used to similar effect. When a heterostructure is grown on a (001) substrate, steps will be present both from the never-perfect orientation of the substrate surface and from islands associated with the growth process [21]. When an interfacial layer is formed on top of such a step, it can be observed clearly in XSTM as an atomically-abrupt shift of the interface, as seen in Fig. 2c. The key to using these ‘steps’ for interfacial analysis comes from recognizing that the underlying steps on the growth surface are

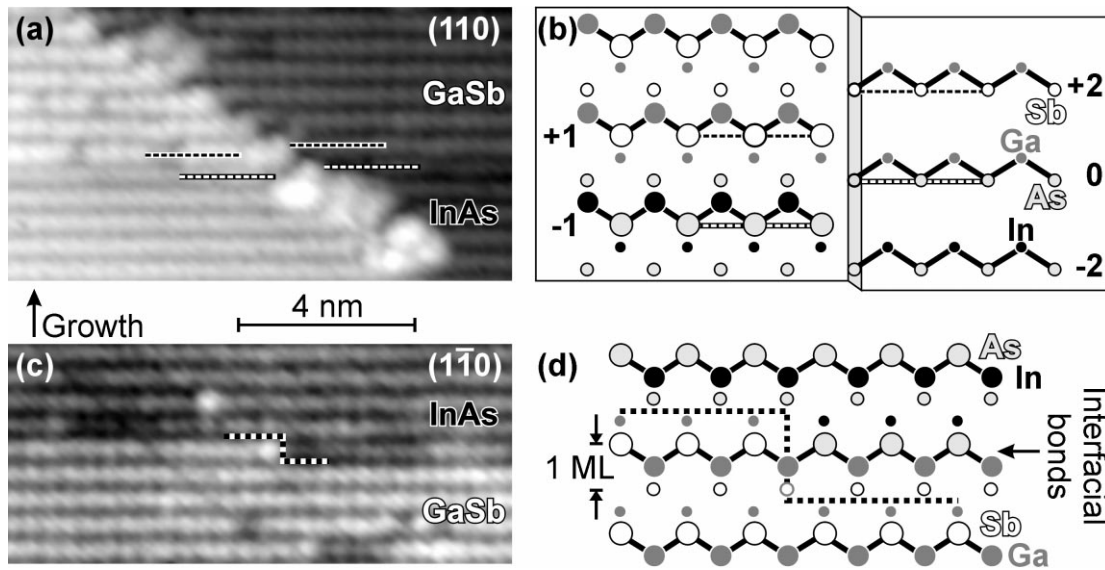


Fig. 2. (a) Filled-states XSTM image of a GaSb–InAs heterostructure where there is a single atomic layer-high step on the (110) cleavage surface. Note that the rows shift by half a unit cell when they cross the step. (b) A structural model illustrating how the alternate growth layers are exposed on either side of the step. The relative position of the interface allows one to identify which is the GaAs interfacial bond layer (denoted as ‘0’) and, by reference, the other layers surrounding the interface. (c) Filled-states image of a $(1\bar{1}0)$ surface showing how a growth step at an InAs-on-GaSb interface appears in XSTM. (d) A structural model of the step, demonstrating how single III–V layer-high growth steps can be used to identify the interfacial layer.

virtually always a *single III–V layer high*. As illustrated in Fig. 2d, because the cross-sectional view shows every-other layer, and in this case the GaAs interfacial layer is above the GaSb, we can deduce that the As-like side of the row on the right side of the ‘step’ must be the interfacial layer. Like the cleavage steps, we find that these steps make it possible to determine the position of the interfacial layer and thereby construct an accurate picture of the atomic-scale structure.

4.2. Spectral analysis of interfacial roughness

The morphological roughness associated with steps on the growth surface may be the most important source of interfacial disorder and has therefore been a prime focus of XSTM studies. One can often use the natural contrast between the heterostructure layers to trace two-dimensional profiles of the interfaces, which can then be digitized and analyzed. Because the effects of interfacial disorder on transport are strongly dependent on the length scale, a common method to charac-

terize the roughness is to calculate the power spectral density of each profile, $|A_q|^2 L$, where A_q is the roughness at wavevector q , and L is the interface length. The spectral density is then fit to a Lorentzian function:

$$|A_q|^2 L = \frac{2\Lambda\Delta^2}{1 + q^2\Lambda^2} \quad (1)$$

to provide a measure of the overall roughness, Δ , and the correlation length, Λ [4–10]. However, it is crucial to recall that, because XSTM only ‘sees’ every other layer (not necessarily including the interfacial layer), *it is impossible to directly measure the true interfacial profile*. To our knowledge, this important limitation to spectral analysis of interfacial roughness has never been discussed in the literature.

When the interfacial roughness is on the order of a few growth layers, the discrepancy between the XSTM profile and the true interfacial structure can be substantial, as detailed in Fig. 3. To demonstrate this discrepancy, we have simulated XSTM

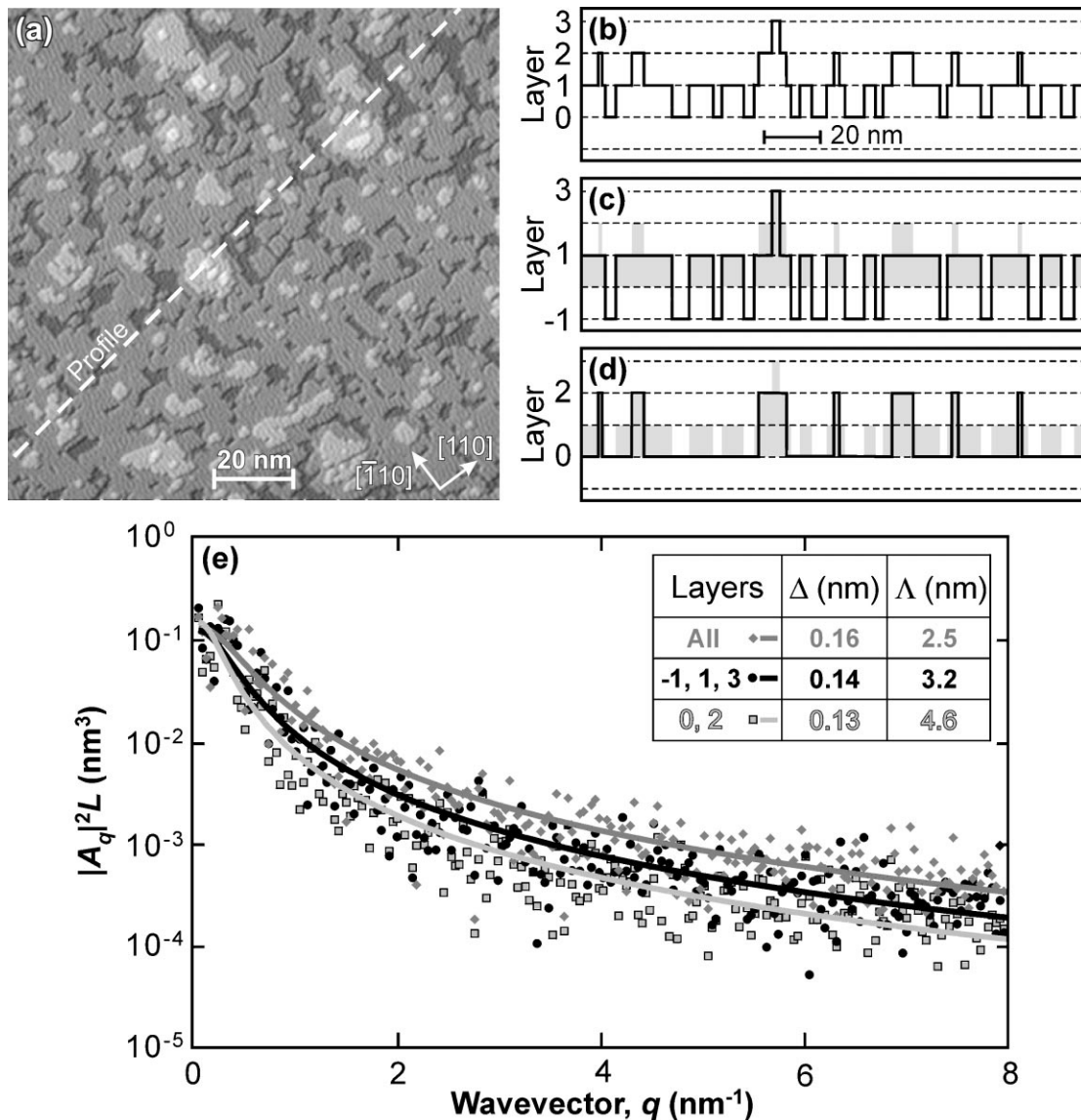


Fig. 3. (a) Plan-view STM image of a 5 ML AISb film grown on InAs. Each layer observed is 1 ML thick (0.3 nm). (b) Profile of the surface topography as indicated on the image. If this surface topography was preserved at an interface, and the resulting interfacial profile observed by XSTM, the profiles shown in (c) and (d) would be measured (the original profile is included in each for comparison). (c) How the profile would look if the cleave exposed the layers above and below the interface, that is, the ‘odd’ layers. (d) How it would look if the ‘even’ layers were exposed. (e) Power spectral density analysis showing the averaged results for five different profiles similar to those shown. The roughness, Δ , and the correlation length, Λ , from the fit to Eq. (1) are shown in the inset for each data set.

interfacial profiles using the actual surface topography of a 5 ML thick AISb film grown on InAs (characterized with plan-view STM) [22]. A profile of the topography along the [110] direction

appears as a series of monolayer-high steps, giving a cross-sectional view of the islands, which typically range from ~ 1 to 20 nm in diameter (Fig. 3b). Neglecting any contributions to the

XSTM profile from compositional intermixing, this profile should be a reasonable representation of the shape of the interface created by deposition of the next material layer. Depending on which layer ends up on the $(1\bar{1}0)$ surface, however, the interface as viewed by XSTM will have one of two possible profiles. Following the notation defined above, the XSTM profile will either show the ‘odd’ growth layers, $-1, +1, +3, \dots$ (Fig. 3c), or the ‘even’ ones, $0, +2, \dots$ (Fig. 3d).

Comparing the alternate-layer profiles (Fig. 3b and c) with the true profile (Fig. 3d), a variety of artifacts are readily apparent. By observing only every other layer, XSTM misses many of the smaller features, so the lateral distance between ‘islands’ appears to increase. Furthermore, the feature heights appear larger on average because all ‘steps’ appear to be two growth layers high. These artifacts show up clearly in the spectral analyses of the profiles, as shown in Fig. 3e. After averaging the power spectra of five different (001) surface profiles to improve statistics, the power spectra for the three cases (odd, even and true profiles) were fitted to the Lorentzian function. The values for Δ and Λ are summarized in the inset. Although the roughnesses only modestly differ in this example, the correlation lengths for the simulated XSTM profiles are significantly larger than the true value. Hence, use of these profiles to model the effects of interface scattering on electrical transport would be spurious. For instance, calculations have shown that the correlation length is perhaps a more important parameter than the magnitude of the interfacial roughness for determining transport in resonant tunneling diode structures [23].

It does not appear that XSTM profiles from both even and odd layers can be combined in any way to reconstruct a true representation of the interfacial roughness power spectrum, because the profiles will always be uncorrelated with respect to the actual structural features. However, our analysis indicates that when the roughness spans four or more growth layers (as appears to be the case for most studies to date), the XSTM profiles begin to provide a reasonable measure of the interfacial structure. Even in these cases, one should keep in mind that it is necessary to acquire roughness data on both the (110) and $(1\bar{1}0)$ sur-

faces because the true roughness is a three-dimensional problem. For example, III–V semiconductor epitaxy often results in anisotropic island shapes, and previous work has demonstrated that this anisotropy can be observed in XSTM measurement of roughness on the two different cleavage surfaces [9].

5. Interpreting images of interfacial bonds

An accurate interpretation of interfacial structure requires an understanding of how to identify atomic-scale features near interfaces in XSTM images, so that the interface can be correctly delineated and the degree of intermixing determined. Taking advantage of the methods described in Section 4.1 to identify the interfacial layers, we have examined how the appearance of these layers depends on the cleavage plane and the heterostructure growth order.

Images of a GaSb–InAs heterostructure specifically incorporating both InSb and GaAs interfacial bonds that were grown in both orders – InAs-on-GaSb and GaSb-on-InAs – are shown in Fig. 4. The Sb or As layer constituting the group-V side of each interface (i.e. layer ‘0’) is indicated. When a distinct contrast is observed for these layers, the Sb row in each InSb layer appears higher (‘brighter’) than the adjacent rows in the GaSb, and the As row in each GaAs layer appears lower (‘darker’) than the adjacent rows in the InAs. In both cases the height difference is ~ 0.02 nm. The GaAs interfaces are generally more disordered than the InSb ones, which are relatively more uniform and abrupt (a phenomenon unrelated to image contrast), consistent with previous characterizations of similar heterostructures [18–20,24,25]. Interestingly, the row contrast is only observed at every other interface; for example, for the InSb interfacial bonds in Fig. 4a, the Sb rows at the InAs-on-GaSb interfaces appear brighter, but those at the GaSb-on-InAs interface look ‘normal.’

The relative image contrast is generally consistent with a simple electronic interpretation based on the bulk properties of III–V bonds. A GaAs bond is less ionic than an InAs bond, so one might expect relatively less charge transfer from Ga to

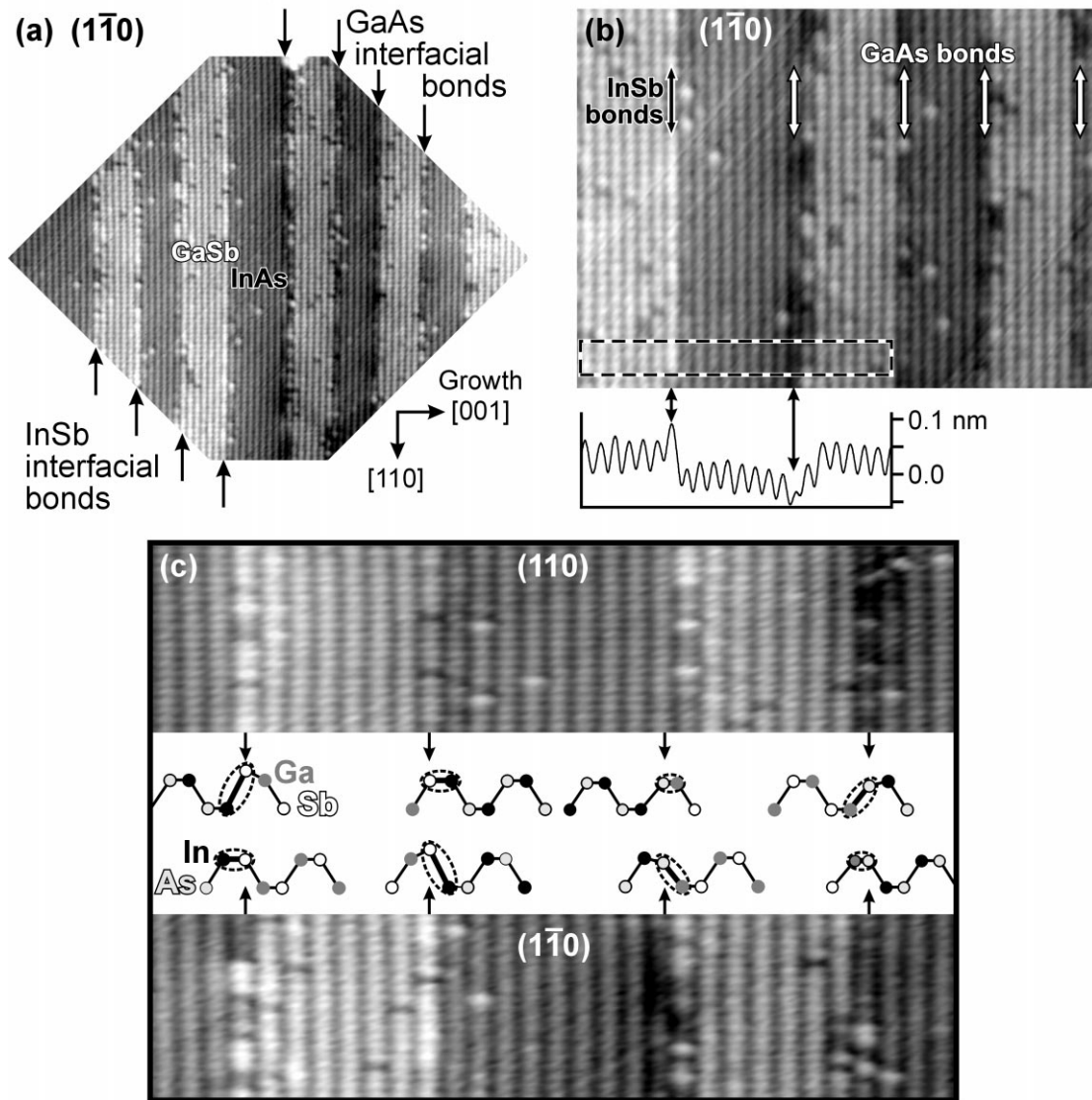


Fig. 4. (a) Filled-states XSTM image, 46 nm across, showing two sets of GaSb–InAs–GaSb structures, one with InSb interfacial bonds and the other with GaAs bonds. (b) Higher magnification view, 23 nm \times 15 nm, highlighting the topographic contrast observed at the interfaces. The average profile is shown from within the region indicated. (c) Images of the heterostructure on both cleavage faces, (110) (top), and $(1\bar{1}0)$ (bottom). The images, 19 nm \times 9 nm, have been compressed by 50% along the row direction to emphasize the row-to-row contrast. Ball-and-stick models (side view) of the surface bond geometry of each interface illustrate how interfacial bond length can account for the topography observed in XSTM. The interfacial bond length differences are exaggerated for clarity.

As, and therefore a lower topographic height in filled-state XSTM images of the associated As row. Conversely, the InSb bond is more ionic than GaSb, which could account for the raised appearance of its Sb row. Additional electronic contribu-

tions to the contrast might also come from shifts in the band edge alignments that are known to occur at the different interfaces. Similar asymmetries have been observed at GaAs/AlAs versus AlAs/GaAs interfaces that appear to be well

accounted for by such electronic contrast mechanisms [15]. However, if the interfacial contrasts in our case were due primarily to electronic effects, we would expect *all* the Sb and As atoms within the interfacial layers to be uniformly affected in the XSTM images. That only half the interfacial layers look different suggests an alternate contrast mechanism in this two-anion case: geometric structure differences, specifically, different bond lengths within the InSb and GaAs interfacial layers.

It is well known that InSb (GaAs) interfacial bonds increase (decrease) the average lattice constant in an GaSb–InAs superlattice [26,27]. Within the heterostructure, these bonds will be strained along $\{110\}$ directions because they must be matched to the surrounding lattice. On the cleavage surface, however, they will be free to relax outward (inward). If the resulting III–V bond length changes are confined to the interfacial layers, the associated XSTM contrast would depend on the orientation of those bonds at the $\{110\}$ surface (see Figs. 1 and 4c). When the bonds are nominally out of the surface plane, the length change would primarily affect the *height* of the atoms on the surface. Using purely geometric considerations and the bulk III–V bond lengths, one would expect the Sb row in an InSb layer to be 0.015 nm higher than on GaSb, and the As row in GaAs the same distance lower than on InAs. These differences are close to what we (easily) observe experimentally. For in-plane interfacial bonds, the length change would be reflected in the lateral distance between the interfacial and adjacent Sb or As rows on the $\{110\}$ surface. A simple geometric analysis shows the inter-row spacing (nominally 0.61 nm) should change by only 5 pm ($<1\%$), a lateral shift that would be very difficult to detect with STM. Therefore, because the bond orientation alternates between interfaces, as discussed in Section 2 and illustrated in Fig. 1, the interfacial bond length differences are only observed with XSTM at every other interface.

A direct test of the contribution of bond length differences to interfacial bond contrast can be made by comparing the contrast on the two $\{110\}$ cleavage surfaces, where the relative bond orientations are reversed. As shown in Fig. 4c, the Sb and As interfacial rows that look different on a $(\bar{1}\bar{1}0)$ surface look like normal GaSb and InAs rows on

a (110) surface, and vice versa. This reversal confirms our proposal that the interfacial bond contrast in these heterostructures is caused primarily by the local geometric, not electronic, structure.

Our experimental results are further supported by first-principles calculations of the equilibrium surface structure on cleaved GaSb–InAs heterostructures, which inherently take into account both geometric and electronic effects, including relaxation at the $\{110\}$ surface [28]. The calculations show that atomic-scale changes in the contours of constant integrated charge density at the interfaces (essentially what is measured by STM) are associated almost completely with local differences in the relative heights of the interfacial Sb or As atoms, in quantitative agreement with our experiments. Moreover, the calculations reveal that geometric distortions also dominate the contrast for point defects, such as an isolated Sb atom in an As lattice site. In contrast, the calculations show that the apparent ‘height’ difference between the GaSb and InAs layers, in general, is mostly associated with electronic structure. For systems where all bonds, including interfacial bonds, are lattice-matched (e.g. GaAs–AlAs), electronic contrast mechanisms will clearly dominate, even at the interfaces. However, when significant bond-length variations are present, our results show that geometric effects will contribute significantly to the contrast between atomic-scale features.

6. Designing heterostructures for optimal interface characterization

To this point, we have identified methods to locate the interfacial layers and interpret the atomic-scale contrast observed. In order to observe both the ‘even’ and ‘odd’ numbered layers surrounding an interface, however, different areas of the surface where these layers were fortuitously exposed by the cleave must be located. This difficulty can be ameliorated by careful design of a model heterostructure; specifically, each structure of interest should be grown in duplicate *separated by an odd number of III–V layers*. For layer-by-layer growth conditions, cleavage will then expose the ‘even’ layers on one of the structures, and the ‘odd’ layers on the other, enabling the observation

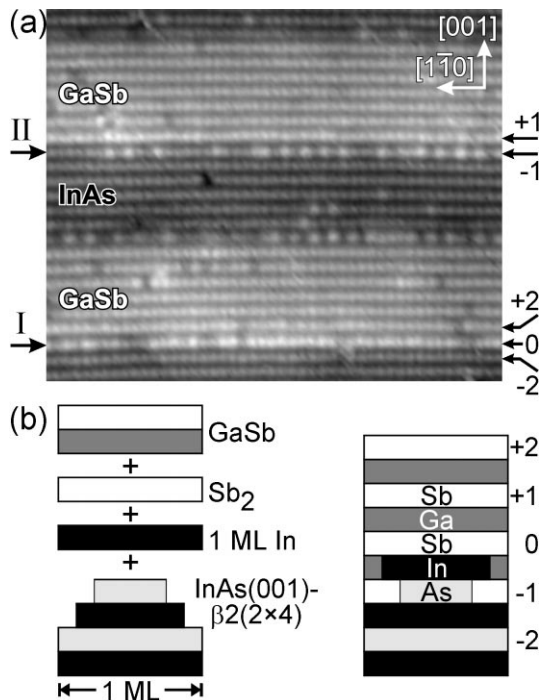


Fig. 5. (a) Filled-states image ($20 \text{ nm} \times 15 \text{ nm}$) of the (110) surface of a GaSb–InAs heterostructure with InSb interfacial bonds. The two interfacial bond layers, labeled ‘I’ and ‘II,’ were separated by an odd number of growth layers so that the ‘even’ layers would be observable at one interface and the ‘odd’ layers at the other. (b) The atomic-scale composition of the interfacial layers are determined by the surface reconstructions during growth, as indicated for InSb interfacial bonds formed by MEE on an InAs(001)- $\beta 2(2 \times 4)$ surface. The resulting layers, including a composite As + Sb layer (‘–1’), are illustrated on the right.

of all the growth layers in a single XSTM image. We have implemented this design scheme in a GaSb–InAs heterostructure with InSb interfacial bonds, as shown in Fig. 5. In this structure, started on an InAs(001)- (2×4) surface, the first GaSb layer consists of the following: 1 ML of In terminated with Sb (InSb bond layer ‘I’); 14 ML of GaSb terminated with Sb; 1 ML of In (InSb bond layer) terminated with As; and 11 ML InAs terminated with As. The second GaSb layer was then grown the same way, beginning with InSb bond layer ‘II’ and ending with a thicker InAs film (only part of which is seen). Because of the V-rich growth conditions, the number of group-III layers determined the film thickness, putting the two GaSb-on-InAs interfaces 27 growth layers apart.

In previous work, we have studied the formation of InSb bonds on InAs(001)- (2×4) surfaces using plan-view STM [22,29,30]. We can now use what we have learned about interpreting XSTM images to build upon our previous understanding of anti-monide–arsenide interfacial bond formation. It is apparent that the roughness at the interfaces can be substantially different depending on which of the two is observed. For interface I, we observe a very abrupt interfacial layer that can now be clearly identified as the raised Sb in out-of-plane InSb bonds (layer ‘0’), with only occasional GaSb-like Sb features. In contrast, the row at interface II is relatively heterogeneous, with an approximately equal mixture of Sb and As-like features. This row can be identified as the last As layer onto which the InSb bond layer was then deposited (layer ‘–1’).

The relative disorder in the last As layer is consistent with our previous understanding of the antimonide-on-arsenide interface. The initial InAs(001)- $\beta 2(2 \times 4)$ surface reconstruction has a non-stoichiometric composition of 0.5 ML As on top of 0.75 ML In, as illustrated schematically in Fig. 5b. The procedure used for forming InSb bonds by MEE – depositing 1 ML of In, followed by a 2 s exposure of Sb_2 and then GaSb growth – cannot result in an abrupt interface. Because of the 0.25 ML of In ‘missing’ from the InAs starting surface, only three-quarters of the MEE layer can form InSb bonds [30]; the remaining interfacial layer must be composed of GaSb. Although this intermixing would be more directly apparent in empty-state images, it does account for the GaSb-like segments of layer ‘0.’ Similarly, the original 0.5 ML of As below the MEE layer must be completed somehow. From the appearance of layer ‘–1,’ we conclude that the As is supplemented by 0.5 ML of Sb, and that the MEE procedure effectively traps this As and nominally inhibits group-V exchange, as intended.

7. Conclusions

Using model GaSb–InAs heterostructures, we have systematically examined how XSTM can be used for the study of III–V heterostructure inter-

faces. We have discussed methods for identifying the location and composition of the interfaces, and the limitations of the technique imposed by both the imaging process and the zinc-blende crystal structure. The interpretation of interfacial structure is impeded by the fact that only every-other III or V plane as grown on the (001) substrate is seen in each image. This structural artifact has significant implications for spectral analyses of interfacial roughness, preventing an accurate analysis for interfaces that are just a few layers wide. Additional complications arise due to the in-equivalence of the (110) and (1 $\bar{1}$ 0) cleavage surfaces and the dependence of interfacial bond orientation on growth order. By taking advantage of the different bond orientations on the two cleavage surfaces, we have shown that the contrast observed at interfacial layers can be an artifact solely of the geometry of the interfacial bonds. Hence, how interfacial bonds appear in XSTM images is a function of bond type, growth order and cleavage plane. Finally, we have shown how this information can be applied to heterostructures grown in pairs with odd atomic layer spacing to simultaneously observe and identify all the growth layers in a heterostructure.

Acknowledgements

This work was supported by the Office of Naval Research, and NRC/NRL Postdoctoral Research Associateships (BZN and WB-C).

References

- [1] P. Roblin, R.C. Potter, A. Fathimulla, *J. Appl. Phys.* 79 (1996) 2502.
- [2] Z.-Y. Ting, T.C. McGill, *J. Vac. Sci. Technol. B* 14 (1996) 2790 (and references therein).
- [3] M.S. Daly, D.M. Symons, M. Lakrimi, R.J. Nicholas, N.J. Mason, P.J. Walker, *Semicond. Sci. Technol.* 11 (1996) 823.
- [4] R.M. Feenstra, D.A. Collins, D.Z.-Y. Ting, M.W. Wang, T.C. McGill, *Phys. Rev. Lett.* 72 (1994) 2749.
- [5] R.M. Feenstra, D.A. Collins, D.Z.-Y. Ting, M.W. Wang, T.C. McGill, *J. Vac. Sci. Technol. B* 12 (1994) 2592.
- [6] J. Harper, M. Weimer, D. Zhang, C.-H. Lin, S.S. Pei, *Appl. Phys. Lett.* 73 (1998) 2805.
- [7] J. Harper, M. Weimer, D. Zhang, C.-H. Lin, S.S. Pei, *J. Vac. Sci. Technol. B* 16 (1998) 1389.
- [8] K.-J. Chao, N. Liu, C.-K. Shih, D.W. Gotthold, B.G. Streetman, *Appl. Phys. Lett.* 75 (1999) 1703.
- [9] A.Y. Lew, S.L. Zuo, E.T. Yu, R.H. Miles, *Appl. Phys. Lett.* 70 (1997) 75.
- [10] A.Y. Lew, S.L. Zuo, E.T. Yu, R.H. Miles, *Phys. Rev. B* 57 (1998) 6534.
- [11] B. Engels, P. Richard, K. Schroeder, S. Blügel, P. Ebert, K. Urban, *Phys. Rev. B* 58 (1998) 7799 (and references therein).
- [12] H. Chen, R.M. Feenstra, R.S. Goldman, C. Silfvenius, G. Landgren, *Appl. Phys. Lett.* 72 (1998) 1727.
- [13] R.M. Feenstra, *Physica B* 273/274 (1999) 796.
- [14] M.B. Johnson, U. Maier, H.-P. Meier, H.W.M. Salemink, *Appl. Phys. Lett.* 63 (1993) 1273.
- [15] A.R. Smith, K.-J. Chao, C.K. Shih, Y.C. Shih, K.A. Anselm, B.G. Streetman, *J. Vac. Sci. Technol. B* 13 (1995) 1824.
- [16] A.S. Bracker, B.R. Bennett, M.J. Yang, J.C. Culbertson, unpublished data.
- [17] M.J. Yang, W.J. Moore, C.H. Yang, R.A. Wilson, B.R. Bennett, B.V. Shanabrook, *J. Appl. Phys.* 85 (1999) 6632.
- [18] B.R. Bennett, B.V. Shanabrook, E.R. Glaser, *Appl. Phys. Lett.* 65 (1994) 598.
- [19] B.R. Bennett, B.V. Shanabrook, R.J. Wagner, J.L. Davis, J.R. Waterman, M.E. Twigg, *Solid-State Electron.* 37 (1994) 733.
- [20] M.E. Twigg, B.R. Bennett, B.V. Shanabrook, J.R. Waterman, J.L. Davis, R.J. Wagner, *Appl. Phys. Lett.* 64 (1994) 3476.
- [21] J.Y. Tsao, *Materials Fundamentals of Molecular Beam Epitaxy*, Academic Press, Boston, 1993.
- [22] B.Z. Noshu, W.H. Weinberg, W. Barvosa-Carter, A.S. Bracker, R. Magno, B.R. Bennett, J.C. Culbertson, B.V. Shanabrook, L.J. Whitman, *J. Vac. Sci. Technol. B* 17 (1999) 1786.
- [23] D.Z.-Y. Ting, T.C. McGill, *J. Vac. Sci. Technol. B* 14 (1996) 2790.
- [24] B. Brar, J. Ibbetson, H. Kroemer, J.H. English, *Appl. Phys. Lett.* 64 (1994) 3392.
- [25] J. Schmitz, J. Wagner, F. Fuchs, N. Herres, P. Koidl, J.D. Ralston, *J. Cryst. Growth* 150 (1994) 858.
- [26] B.R. Bennett, B.V. Shanabrook, R.J. Wagner, J.L. Davis, J.R. Waterman, *Appl. Phys. Lett.* 63 (1993) 949.
- [27] J. Wagner, J. Schmitz, N. Herres, F. Fuchs, D. Serries, B. Grietens, S. Németh, C.V. Hoof, G. Borghs, *Physica E* 2 (1998) 320.
- [28] S.-G. Kim, B.Z. Noshu, L.J. Whitman, S.C. Erwin (in preparation).
- [29] B.Z. Noshu, W.H. Weinberg, J.J. Zinck, B.V. Shanabrook, B.R. Bennett, L.J. Whitman, *J. Vac. Sci. Technol. B* 16 (1998) 2381.
- [30] B.Z. Noshu, W.H. Weinberg, W. Barvosa-Carter, B.R. Bennett, B.V. Shanabrook, L.J. Whitman, *Appl. Phys. Lett.* 74 (1999) 1704.